Experimental investigation of bladeless expander with an incompressible fluid

Experimental investigation of bladeless expander with an incompressible fluid

Avinash Renuke[1], Federico Reggio[2], Matteo Pascenti[1] and Alberto Traverso[1]

[1]Thermochemical Power Group (TPG), University of Genoa, Italy
via montallegro 1, Genoa – 16145, Italy

[2]SIT Technology srl, Genoa, Italy

renukeavinash@gmail.com

Abstract. For small-medium heat pumps and small-scale energy storage (e.g., hydro) and other small-scale applications (up to 10kWe), an economical, reliable, durable, robust, and acceptable performing bladeless expander is an attractive technology. In this article, experiments are performed on a bladeless expander of 1kW design power with water as a working fluid. The complete expansion is in the subcooled liquid phase with an overall pressure drop across the expander in the 2-14 bar range. The water expander is designed as a similitude case study for a butane heat pump, where such a bladeless expander could replace the expansion valve recovering untapped energy from isenthalpic to isentropic expansion. Unlike conventional bladed expanders, the present bladeless expander consists of several co-rotating compact disks, closely spaced and parallelly mounted on the shaft which transmits torque using wall shear forces. The present expander design is an improved version resulting from the detailed loss characterisation done on earlier air expanders.

The article begins with the definition of design conditions for water expander starting from the expected butane expansion in the heat pump, fully inside the liquid region. The rotor design of a bladeless expander is outlined using dimensionless parameters that dictate the performance features. The turbine is designed for 1kW of power output and 2kg/s mass flow with an overall pressure drop of 14 bar with a rotational speed of 8000 rpm. The resulting turbine rotor consists of an 80mm disk outer diameter, 120 disks and a 0.1mm gap between them. An experimental test rig employing water as a working fluid is described. Experiments are conducted for overall pressure drop ranging in the 2-14 bar interval, with a maximum rotational speed of 6500 rpm. The performance is recorded with two different stator configurations, having two different throat dimensions for varying mass flow at maximum inlet pressure. Peak total to static efficiency of 30% is obtained with a net power of 670 W at ~3000 rpm. An experimental ventilation loss (end wall viscous disk friction) is performed with both water and air as working fluids to estimate the power loss. It is found that ventilation loss is the major source of loss in the present turbine prototype with a power loss of 250W@3000 and 1100W@8000 rpm, varying quadratically with rotational speed. It is finally concluded that the expander performance is promising because ventilation losses can be potentially reduced with established strategies used in conventional expanders.

1. Introduction

Bladeless turbomachines, also known as Tesla turbomachines, were invented by Nikola Tesla in the early 19th century [1][2]. It consists of thin disks with a central hole, mounted parallel on the shaft with spacing between them. In turbine mode, fluid enters tangentially to the rotor and leaves the rotor at the central hole axially. In a compressor mode, fluid enters from the central holes of the disks and leaves from the periphery. The peripheral high-speed is then converted into static pressure using external volute. Hence, this machine is reversible – by changing the rotational direction of the rotor both the modes, turbine and compressor, can be operated using a single machine. The relative velocity between fluid and the disk is very low compared to conventional bladed turbines. Due to the lower relative velocity, the flow inside the rotor is laminar. The laminar flow field inside the Tesla turbine rotor is the key to the effective energy transfer between fluid and the disk. The fluid layers between the gap of the disks transfer energy through shear force. This energy exchange between the fluid layers and between the last fluid layer to the disk is due to shear force. The drag force generated on the disk due to this shear is in the direction of rotation of the disk. Hence, in the case of Tesla rotor, viscous shear drag is in favour of power generation unlike a loss in the case of bladed turbines, where viscous drag is in the opposite direction of rotor propulsion. This interesting phenomenon has attracted many researchers to study bladeless turbines.

Tesla claimed to have very high rotor efficiency (up to 97%) [3]. This has also been proved by researchers analytically as well as numerically [6-18]. However, experimentally the complete Tesla turbine efficiency (stator + rotor) has been found very low (< 35%) [4][5], but still interesting for energy harvesting, storage, or small ORC [19] applications.

The power recovery in the refrigeration and heat pumps using the Tesla turbine has been patented by Authors [2] and demonstrated in the literature as well as at the University of Genoa laboratories. However, the efficiency of the turbine evaluated experimentally was found to be low. In this study, we perform the bladeless expander experimental investigation for heat pump application representative conditions, considering a butane heat pump where expansion occurs fully in the subcooled liquid region, therefore allowing for applying incompressible fluid similitude when operating with water.

The key role of the Tesla expanders-assisted heat pumps is to improve the system level efficiency and to recover energy economically. The proposed solution utilizes the pressure difference between the condenser and evaporator employing an expander to produce useful power. This expansion is theoretically isentropic (Figure 1(right) – CD'). The introduction of an expander into the system reduces the consumption of mechanical energy of the compressor and reduces the quality (vapour mass fraction with respect to the total mass in liquid and vapour phases) of the working fluid at the inlet of the evaporator, thus increasing the available enthalpy difference (h_A-h_D') from evaporator inlet to evaporator outlet. The increase in the performance of the heat pump can be measured by an increase in the coefficient of performance (COP). COP is defined as the ratio between the heat absorbed by the evaporator and the absolute value of the work that is required by the compressor.

$$COP = (h_A - h_{D'}) / (h_B - h_A) \quad (1)$$

The typical value of COP may range from 2-10 depending upon the application, size and refrigerant.

Both the reduction in mechanical energy and the reduction in quality, thanks to the introduction of a turbine between condenser and evaporator, are known to allow an increase of COP up to 20%. The design point case used to design the prototype object of this investigation is for a thermodynamic state for Butane as shown in Figure 2. The P-h diagram shows the expansion occurring in the liquid phase (incompressible fluid): therefore, in this specific application, it is possible to consider water (safe – incompressible fluid) for laboratory demonstration within similitude conditions, which represents the butane working fluid case.

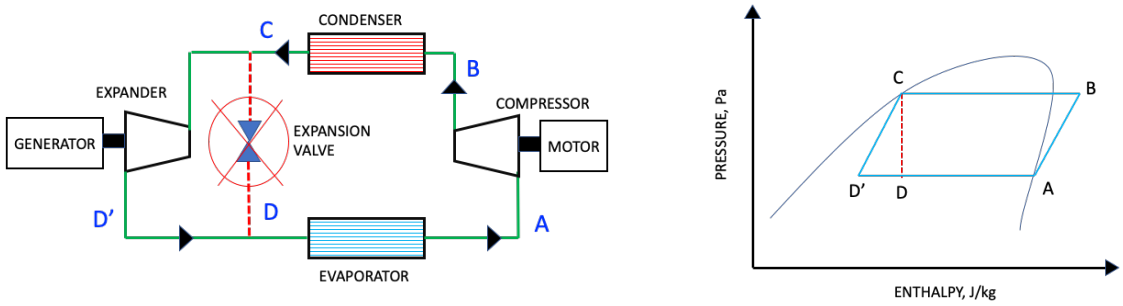

Figure 1 Schematic of reverse Rankine cycle (left) and pressure-enthalpy chart (right)

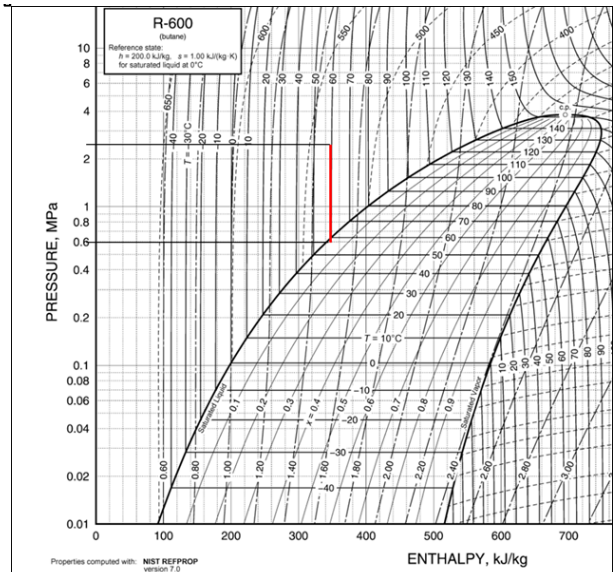

Figure 2 P-h diagram for n-butane (R-600) with design conditions for expander

2. Expander design

In Table 1, requirements and specifications for the prototype operating with water are reported:

Table 1. Thermodynamic design specifications for water

Thermodynamic data	Demonstration design data
Working fluid	Water
dp across turbine, bar	14
Rotational speed, rpm	8000
Mass flow, kg/s	2
Power, W	1400 (expected)
Expected efficiency, %	70+ (without leakage, ventilation and bearing loss)

The selected electrical generator has a rated rotational speed of 10000rpm with 3 kW power, which is considered a starting point for the analysis. The following design procedure is adopted to design the rotor and the stator of the expander.

1. The pressure drop across the expander is used to calculate the exit velocity of the nozzle. The outer diameter for the rotor is calculated for the optimum velocity ratio at the inlet of the rotor.

2. Reynolds number, $Re_{b.b} = (\varrho.b.(b.\omega))/\mu$ [where, ϱ is density (kg/m3), b is gap between disks (m), ω is angular velocity (rad/s) and μ is dynamic viscosity (Pa.s)] of 4 is selected for the calculation of gap between disks. Using the fluid thermodynamics properties, the gap between disks comes out to be 0.1 mm.
3. As a check for similarity parameter, $P = b/2.\text{sqrt}(\omega/\nu)$ [where b is gap between disks (m), ω is angular velocity (rad/s) and ν is kinematic viscosity (m^2/s)], is evaluated. This is close to the recommended value of $\pi/2$ [21].
4. The fluid being of higher density, inner diameter is calculated using a diameter ratio of 2 (outer to the inner diameter of rotor). The diameter ratio of 2 is chosen considering the outlet area blockage due to the shaft and discrete exhaust holes on the disks. The calculated outlet diameter for the rotor is 30 mm.
5. Radial velocity is calculated by setting an inlet flow angle of 1-2 degrees for near tangential flow at the rotor. In this case, an inlet flow angle of 5 degrees is considered for practical reasons. Inlet flow angle is the angle between absolute fluid velocity through the nozzle to the disk tip velocity. Geometrical representation is shown in Figure 3.

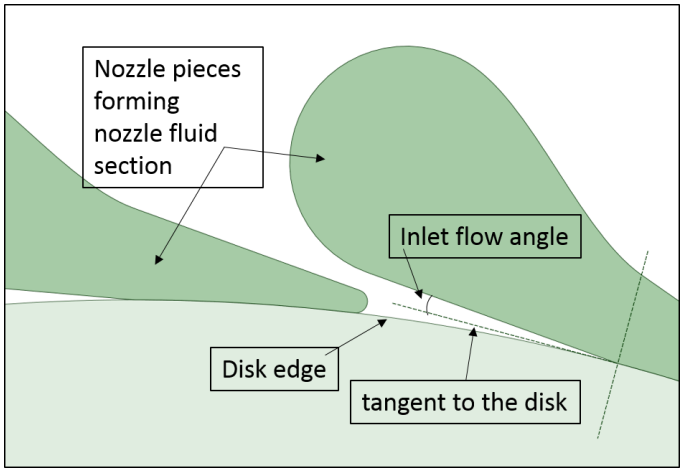

Figure 3 Inlet flow angle between nozzle and rotor represented in 2D drawing

6. Using the radial velocity, mass flow and flow rate per gap are calculated.
7. Flow rate is checked with respect to the flow rate parameter, $q_f = Q/(\omega.r_o\text{^}3) \sim 0.00001\text{-}0.0001$[3], [where, Q is the volume flow rate (m^3/s), ω is the angular velocity (rad/s) and r_o is outer diameter] the calculated flow rate parameter, in this case, is 0.0003 which is in the acceptable range to obtain rotor efficiency higher than 85% [3].
8. Torque per disk is calculated using Euler's equation and power per disk (multiplying torque with angular velocity).
9. The number of disks of 150 is calculated based on total mass flow and mass flow per gap between disks.
10. The efficiency calculated using the ratio of output power and inlet power (analytical) is ~82%.

The geometrical specifications of the turbine prototype for demonstration are reported in Table 2, considering the manufacturing constraints given by 3D printing, employed for the stator ring.

Table 2. Turbine design geometrical parameters

Stator	3D printed nozzles – 5 deg angle
Number of nozzles	24
Rotor disk outer diameter, mm	80
Rotor disk inner diameter, mm	32
Disk discharge section holes	3
Disk thickness, mm	0.1
Disk gap, mm	0.1
Number of disks	150

3. Turbine Components and Test Rig

In this section, the water expander prototype and related experimental set-up are presented. The different components of the water expander can be seen in Figure 4. The turbine consists of the following main components:

Inlet port: inlet port is the inlet piping connection for the water to enter the turbine. Water from the inlet port enters stator/nozzles. There are two inlet ports used in this turbine.
Stator: there are 24 nozzles placed around the circumference of the rotor, which increase the velocity of the incoming water. High-speed jets of water enter the rotor. The stator is manufactured using 3D printing technology into one single piece. Both polymeric, as well as metallic stators, have been printed, to check the feasibility of the proposed design and the precision attainable with different materials. Also, two rotating-shaped disks are incorporated at the rotor end to guide the flow from nozzles into the disk pack.
Rotor: turbine rotor consists of thin metal disks parallelly mounted on the shaft. The disks are separated by spacers, which maintain the desired gap between disks along with rotating-shaped disks, as discussed in the previous chapter.
Radial diffuser: radial diffuser at the exit of the turbine is used to convert the exit kinetic energy of the water into pressure energy.
Collector: the water coming out of the radial diffuser still has tangential velocity and, to redirect the flow into a single channel/pipe, a collector is used. The role of the collector is to smoothly transfer water from the radial diffuser to the exit pipe.
The turbine assembly is started from the motor end. Following is the sequence of the components in the assembly of the machine.

1. Bearings and bushings are inserted into the bearing housing.
2. A stationary end plates are placed which supports the stator ad inlet ports.
3. Seals are introduced and 3D printed nozzle is attached to the end plate
4. Rotor pack is then inserted and aligned together with the shaft.
5. An end plate, forming radial diffuser and exhaust collector is then assembled.
6. All the end plates are then tightened together with the help of studs.

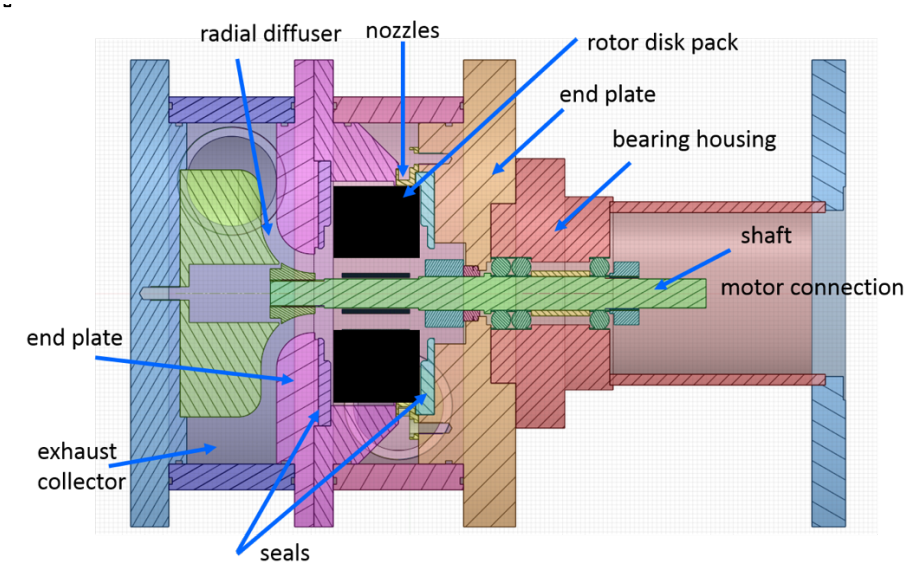

Figure 4 2D drawing of water Tesla expander

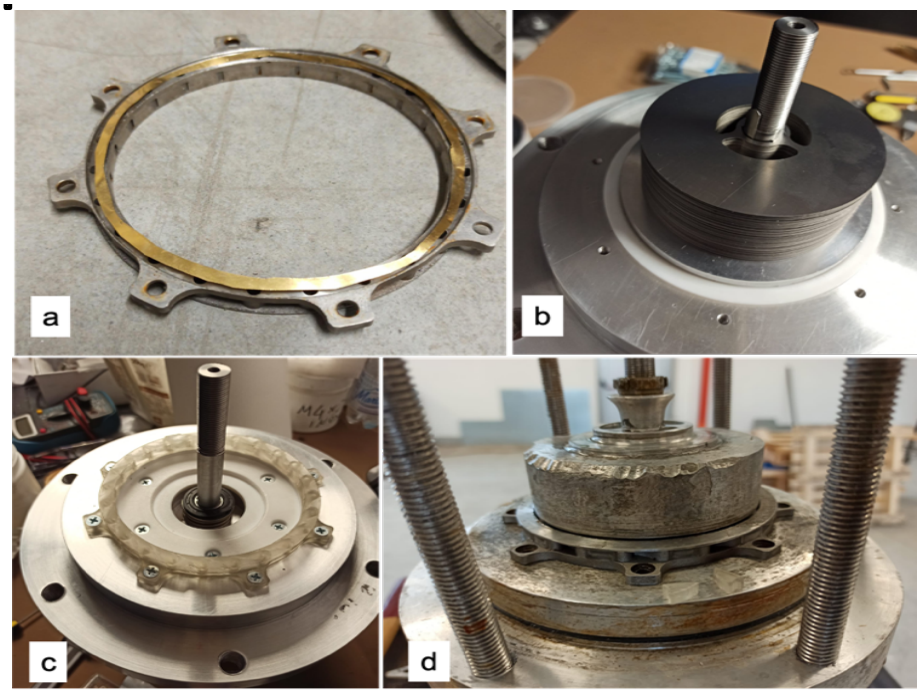

Figure 5 Water Tesla expander components: (a) metallic stator, (b) rotor assembly, (c) rotor with plastic stator, (d) rotor with the metallic stator (balancing removals are visible)

This Tesla turbine was designed to operate at speeds up to 10,000 rpm. Given the need to seal the turbine casing, the rotor has a cantilevered (as shown in Figure 5(b)) arrangement to allow the use of a single mechanical seal. The mechanical seal has been placed to avoid the water exit where the 15mm diameter shaft is coming out of the turbine casing for connecting to the generator through a joint. The rotor is supported by three spindle bearings placed on the generator side between the mechanical seal and the joint, while on the opposite side the cantilevered disk pack is held together by a shaped ring nut. The turbine has 3 chambers: the cylindrical inlet manifold, connected externally to the 2 inlet pipes, surrounds the stator and the chamber containing the rotating disks, finally the liquid that comes out of the turbine is collected in an exhaust manifold and exits from the 2 pipes drain. All the machine

components are kept together by flanges and 6 threaded rods with a 12mm diameter. Figure 5 (c)(d) shows the rotor and stator assembly of the expander.

Figure 6 - Water expander experimental test rig

The inlet pressure to the turbine is provided by a high-pressure water pump to achieve a 14 bar pressure difference between the turbine inlet and turbine exit as shown in Figure 6. Turbine exit is subject to higher than atmospheric pressure due to discharge line pressure drops. The water test rig system is controlled by various valves to control the operation of the system.

To evaluate the performance of the expander, the power and efficiency of the expander are considered the first key indicators.

Power is calculated using torque applied by the electrical rotor (therefore the statoric electrical losses are not considered) and angular velocity as:

$$P = \tau . \omega \tag{2}$$

Such values can directly be obtained by the motor variable speed driver.

Torque is evaluated by measuring the current output of the generator and using the conversion factor given by the generator manufacturer.

$$\text{Torque } (\tau) = \text{current} * 0.344, \text{Nm} \tag{3}$$

Hydraulic efficiency, incorporating the bearing mechanical losses, is computed as follows,

$$\eta = \frac{P}{\frac{\dot{m}}{\rho} \Delta p} \tag{4}$$

where P is power (W), m is the mass flow rate (kg/s), Δp is pressure drop across turbine (Pa) and ρ is density (kg/m^3).

4. Experimental error Analysis

The efficiency of the expander is calculated using Eq. (4), which is evaluated from the measured parameters like pressure, rotational speed, mass flow and current. Each of these quantities is affected by uncertainties due to instrumental error, calibration error, and random error that propagate to the result through the function that binds the result to these parameters. Instrumental errors for digitally recorded values are assumed negligible. Random error is calculated by repeating the experiment under the same atmospheric conditions and with the same user for different rotational speeds and inlet pressure.

Combined error is calculated by using the root sum square method. The uncertainty of a given function g with n direct measures, g = f (x1, x2, x3,..., xn), can be calculated as follows:

$$U_g = \sqrt{\sum_{i=1}^{n} \cdot \left(\frac{dg_i}{dx_i}\Delta x_i\right)^2} \quad (5)$$

where *Ug* is the uncertainty observed in the output of function g, while Δx_i is uncertainty in i^{th} measure. Uncertainty of efficiency is calculated over a broad range of data.

Table 3 shows the uncertainty in the instruments used in the experimental analysis. To account for the 95.5% confidence interval, the standard deviation for all repeated measurements is taken into consideration as ±2 SD. Maximum uncertainty in efficiency and power is found to be ~ ±0.8% and ~ ±30W, respectively.

Table 3 Measurement accuracy of sensors

Sensors	**Range**	**Accuracy**
Turbine inlet pressure	0 - 25 bar	±5%
Turbine exit pressure	0 - 6 bar	±2.5%
Stator and rotor clearance pressure	0 - 16 bar	±2.5%
Mass flow	0 - 5 kg/s	±1.5%
Generator current	0 - 9 A	±0.5%
Rotational speed	0-10krpm	±0.01 %

5. Results

In this section, results of two tests are presented. The first test involves the nozzle with 0.4 mm throat height and the second test is carried out at the nozzle throat height of 0.8 mm. In the first test design flow of 2 kg/s is not achieved due to higher tolerances in 3D printing process. After reviewing the data from first test, new nozzle with higher throat section is introduced to achieve the design flow.

Test 1

Experiments are conducted for various pressure drops across the turbine, i.e. from 2 bar to 15 bar inlet pressures. The 3D printed metallic nozzle used for this test 1 has a design throat height of 0.4 mm. The generator attached to the turbine records rotational speed and current. The power is calculated using the current and torque coefficient (obtained from the manufacturer for the generator used).

Figure 7 shows the cases of the power for 100% and 90% water pump speeds. The dashed line, which is power without ventilation loss (ventilation losses are measured and discussed later), shows increasing trends and may have a peak at higher rotational speeds. It means that the turbine will have high performance if ventilation losses are reduced (which is attainable through conventional solutions).

Similar trends can be seen in the efficiency plots as shown in Figure 8. The dashed lines represent performance without ventilation loss, showing promising higher values. Also, with respect to rotational speeds, these dashed curves tend to show increasing trends for higher rotational speed, i.e., toward the design speed of 10000 rpm.

The trends shown in the experimental results are promising as they indicate, for stator-rotor design regardless of ventilation losses, the possibility of higher performance at higher speed and mass flow. The turbine is designed for a pressure difference of 14 bar, a mass flow rate of 2 kg/s and a rotational speed of 10000 rpm. In the present test 1 campaign, the turbine prototype could not elaborate the design mass flow at a pressure difference of 14 bar. This is due to the undersized nozzles (tolerance errors in 3D printing of metallic nozzles – manufacturing limitation for small nozzle dimensions).

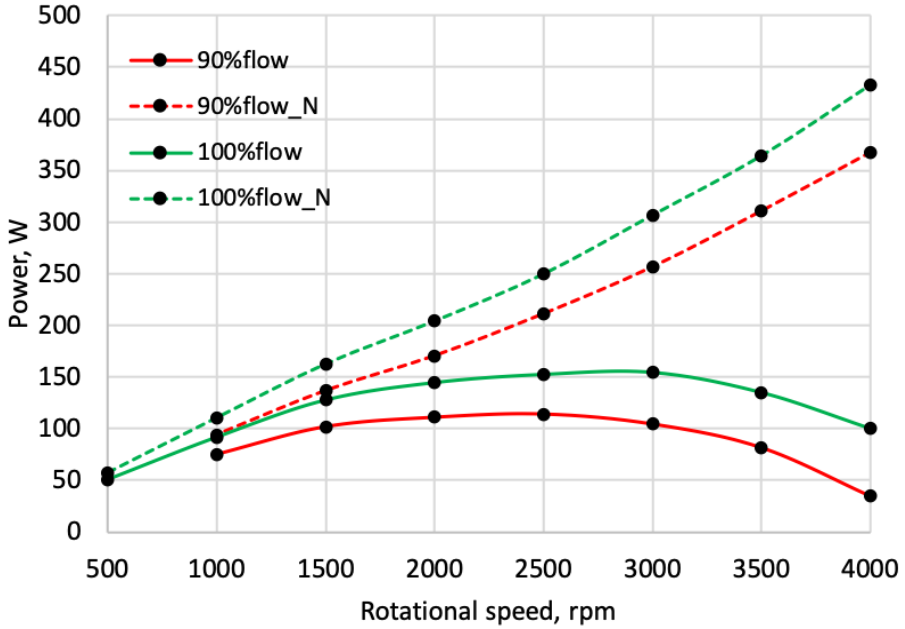

Figure 7 - Mechanical power vs rotational speed at different flows i.e. 90% and 100% of water pump speed (100% pump speed corresponds to approx. 1.1 kg/s mass flow) (dashed lines are estimated w/o ventilation losses)

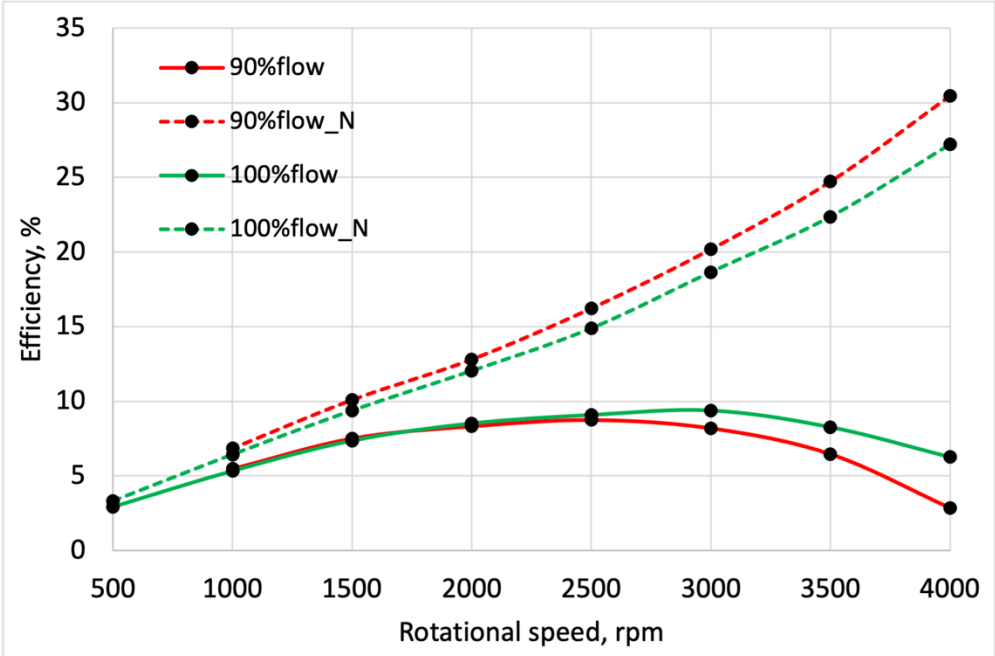

Figure 8 - Efficiency vs rotational speed at different flows i.e. 90% and 100% pump speed (100% pump speed corresponds to approx. 1.1 kg/s mass flow) (dashed lines are estimated w/o ventilation losses)

Test 2

In the previous experimental test, 3D printed metallic nozzles with 0.4 mm throat height were used. This throat section was designed based on the required mass flow and pressure difference. However, in the test, at 14 bar of Δp, a mass flow of 1.1 kg/s was obtained. In the analysis of the prototype, it was found

that due to very small dimensions, 3D metallic printing produced higher tolerances making the effective total nozzle area smaller than the designed one: this was the main cause of the reduced mass flow.
Therefore, in this test 2 the nozzles have been printed in polymeric material with a higher design throat height (~ 0.8mm). In the new test 2, however, no improvements were carried out to tackle the ventilation loss issue to assess the causes separately and systematically.
Figure 9 shows the pressure difference across turbine versus mass flow. It is illustrated that, with the new nozzle, higher mass flow is obtained compared to previous tests for the same Δp. This indicates that the new 3D printed polymeric nozzles may have larger throat sections than the design due to 3D printing tolerances, which increases mass flow by more than double the design values.
New tests were also performed similarly as previously discussed with a new nozzle with 0.8 mm throat height. Figure 10 and Figure 11 show the performance results i.e. efficiency and power versus rotational speed with different mass flows. There is a significant improvement in the performance of the expander reaching maximum efficiency of ~30% (10% in the old test) with a power of 690 W (150 W in the old test).

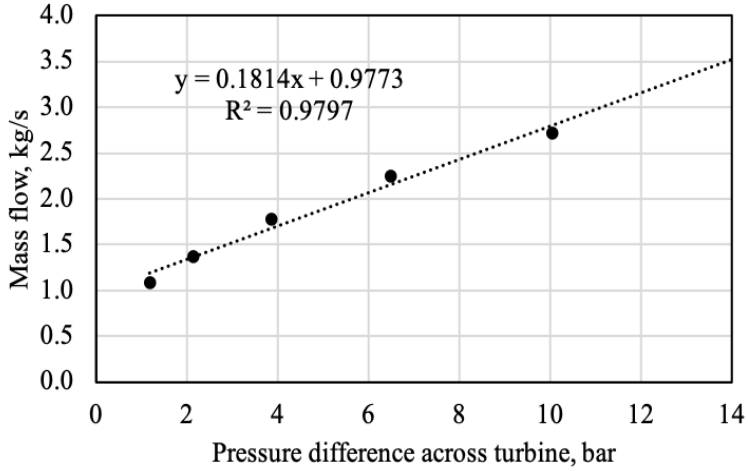

Figure 9- Pressure difference across turbine versus mass flow for Test 2 (in Test 1 maximum mass flow of 1.1 kg/s has been recorded for 14 bar pressure difference)

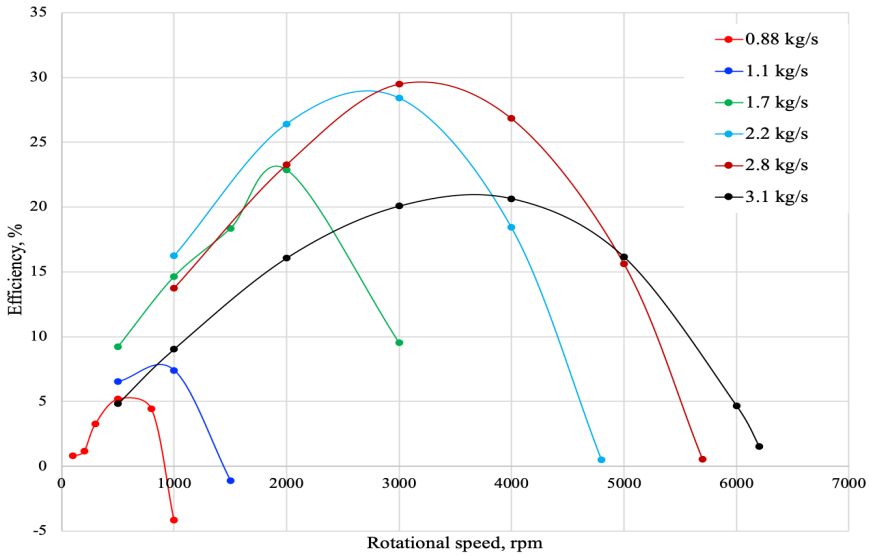

Figure 10 - Efficiency versus rotational speed at different mass flows

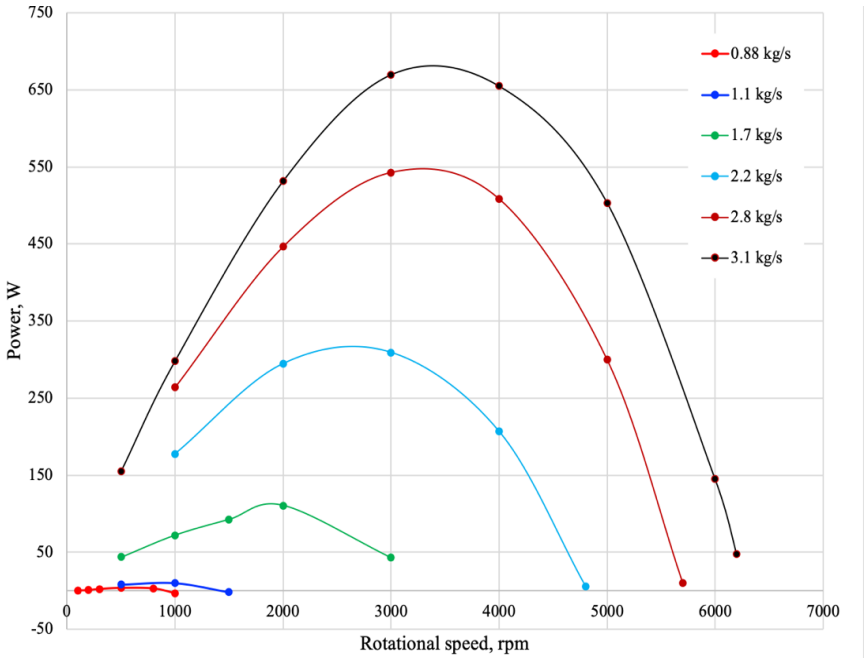

Figure 11- Mechanical power versus rotational speed at different mass flows

Ventilation losses

As per experimental tests, the performance of the water expander was not as expected by numerical results. To understand the cause, as the first intuition for the major source of losses to be ventilation due to the high available surface of rotating parts with respect to casing, a run-down experiment is performed. The run-down experiment is performed both with air (i.e., empty turbine) and water. Run down is started with the rotational speed of 10000 rpm and when the water supply is cut off, the rotor comes to rest due to viscous resistances in the stator-rotor cavity. By considering the balance equation on the rotor shaft, where ventilation losses (and bearing losses) drag power from the rotating inertia, which is known, instantaneous ventilation losses can be estimated by the speed time record. Since the turbine is equipped with an anti-leak system, any pumping effect may be neglected as a first approximation.

Bearing losses constitute a small fraction of all losses, and they could be estimated separately with a similar run-down procedure but having displaced the water with air inside the rotor chamber.

Figure 12 shows the ventilation power loss with respect to rotational speed. The ventilation loss for water shows a strong quadratic trend with respect to rotational speed. We can see that ventilation losses are significant if we compare the design power of the machine, which is 1.4 kW @10000 rpm. The ventilation power loss is greater than the design power. Hence there is no production of positive power at a higher rotational speed.

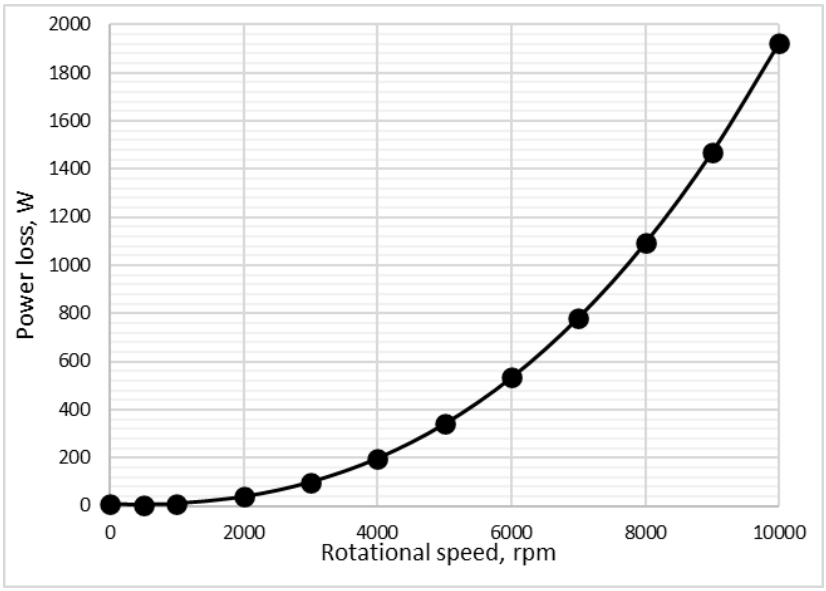

Figure 12 – Measured experimental ventilation losses

Figure 13 shows the experimental performance calculated without ventilation losses. It can be observed that the curves at mass flow 1.7 kg/s and 2.2 kg/s are approaching efficiency higher than 70%. This suggests that if the ventilation losses are reduced, the expander performance matches with numerical performance. In the near future, the validated 2-D model can be further used to optimise and reduce the power loss due to ventilation, applying conventional approaches (e.g. increase in clearance and high surface finish) as well as innovative concepts (e.g. superficial features).

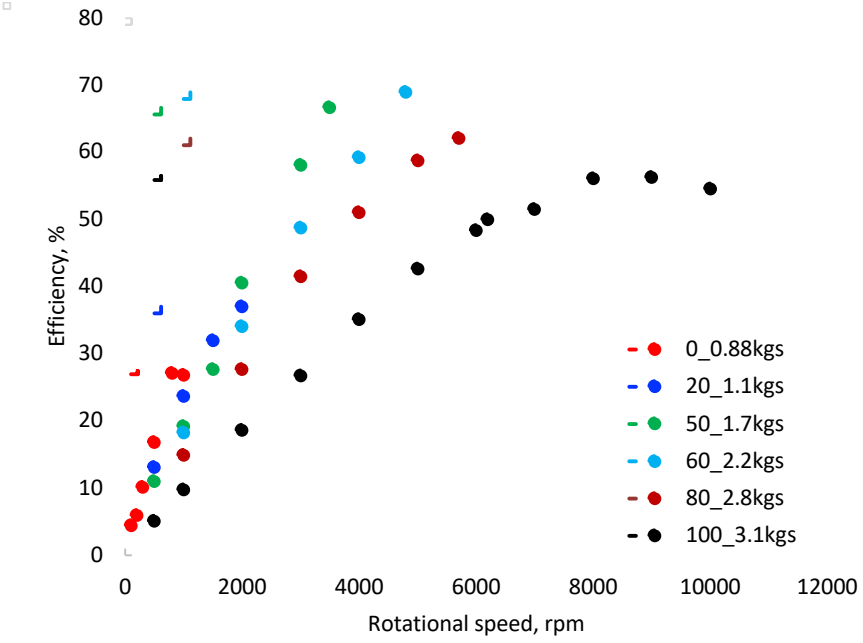

Figure 13 – Estimated experimental performance w/o ventilation losses

6. Conclusions

In this study, design activity and experimental performance characterisation of a bladeless turbine prototype are carried out using water as a working fluid, bringing to the following conclusions:

1. Water expander design and manufacturing: The expander is designed using an in-house 1D design tool. The flow path of the expander is then constructed in CAD software and turbine assembly is made according to previous manufacturing experience. Numerical results of stator and rotor show 70% efficiency at design conditions which is 8000 rpm, 2 kg/s mass flow and pressure difference of 15 bar across the expander.
2. Water expander experimental results: The experimental campaign is performed at design point pressure and off-design conditions for different rotational speeds and pressure drops across the expander. It was difficult to obtain the design mass flow due to the high tolerances of 3D printed nozzles, either metallic (test 1) or polymeric (test 2). The maximum efficiency of 30% is recorded and a maximum power of 660 W at 3200 rpm is obtained. The maximum rotational speed reached by the turbine was 6500 rpm (without power generation). This is mainly due to ventilation losses between end rotating disks and casing. Experimental ventilation loss characterisation is performed to estimate the power lost due to ventilation. Results showed very high ventilation loss, >1 kW @8000 rpm (design speed). Due to very high ventilation losses, the turbine could not reach its design speed. However, the results show that the present design eliminated the traditional stator-rotor losses present in the Tesla machines. The ventilation losses, between rotating end-disks and casing, could be later reduced by traditional approaches.

In the current study, the design performance was still not achieved due to possible following reasons:

i. The turbine is tested in far from design condition due to tolerances in the 3D printed nozzle. At higher mass flow, more than double in this case, the performance of the Tesla rotor drops significantly. Tuning the manufacturing procedure of small throat nozzles is necessary to achieve the design mass flow through the turbine.
ii. Ventilation losses are found to be very high. The power lost due to ventilation is significant, dragging the rotor and preventing the design rotational speed from being achieved. However, it has been demonstrated that the current rotor design allows drawing the expected useful work from the working fluid (i.e. stator/rotor interaction losses have been minimised), but most of the useful work is later dissipated through ventilation.

The performance of the turbine will be investigated soon considering the above-mentioned factors with an improved version of this expander prototype.

References

[1] Tesla, N., 1913, “Fluid propulsion’’ US Patent 1061142
[2] Tesla, N., 1913, “Turbine”, US Patent 1061206.
[3] Rice, W., 1963, “An Analytical and Experimental Investigation of Multiple Disk Pumps and Compressors”, J. Eng. for Power 1963. Pp. 191-198.
[4] Renuke, A., Vannoni, A., Traverso, A., and Pascenti, M., 2019, “Experimental and Numerical Investigation of Small-Scale Tesla Turbines”, *ASME. Journal of Engineering Gas Turbines Power*, Vol. 141(12), 121011.
[5] Renuke, A., Reggio, F., Pascenti, M., Silvestri, P and Traverso, A., 2020, “Experimental Investigation on a 3 kW Tesla Expander with High-Speed Generator”, ASME. TurboExpo’20, GT2020-14572, London, England.

[6] Matsch L., Rice W., "An asymptotic solution for laminar flow of an incompressible fluid between rotating disks", Transactions of the ASME, Journal of Applied Mechanics, 1968.
[7] Boyak B.E., Rice W., "Integral method for flow between corotating disks", ASME Journal of Basic Engineering, 93, 350–354, 1971.
[8] Lawn M.J., Rice W., "Calculated design data for multiple–disk turbine using incompressible fluid", Transactions of the ASME, Journal of Fluid Engineering, 252–258, 1974.
[9] Truman C.R., Rice W., Jankowski D.F., "Laminar throughflow of varying–quality steam between corotating disks", Transactions of the ASME, Journal of Fluid Engineering, 194–200, 1978.
[10] Allen J.S., A model for fluid between parallel, co-rotating annular disks, M.Sc. Thesis, University of Dayton, Ohio, 1990.
[11] Carey V.P., "Computational/Theoretical Modelling of Flow Physics and Transport in Disk Rotor Drag Turbine Expanders for Green Energy Conversion Technologies", Proc. of the ASME 2010 International Mechanical Engineering Congress & Exposition, Vancouver, Canada; 2010.
[12] Puzyrewski R., Tesch K., "1D model calibration based on 3D calculations for Tesla turbine", Task quarterly, scientific bulletin of the academic computer centre in Gdansk, 14, 237–248, 2010.
[13] Batista M., "Steady flow of incompressible fluid between two co-rotating disks",Appl. Mathematical Modelling, 35, 5225–5233, 2011.
[14] Lampart P., Jedrzejewski L., "Investigations of the aerodynamics of Tesla bladeless microturbines", Journal of Theoretical and Applied Mechanic, 49, 2, 477–499, 2011.
[15] Romanin V.D., Krishnan V.G., Carey V.P., Maharbiz M.M., "Experimental and analytical study of a sub–watt scale Tesla turbine performance", Proceedings of the ASME 2012 International Mechanical Engineering Congress & Exposition, Houston, 2012.
[16] Bao G., Shi Y., Cai N., "Numerical modelling research on the boundary layer turbine using organic working fluid", Proceeding of International Conference on Power Engineering (ICOPE–13), Wuhan, China, 2013.
[17] Guha A., Sengupta S., "A non–dimensional study of the flow through co-rotating discs and performance optimization of a Tesla disc turbine", Proc. IMechE Part A: Journal of Power and Energy, 1–18, 2017.
[18] Song J., Gu C.W., "1D model analysis of Tesla turbine for small scale organic Rankine cycle (ORC) system", in: Proceedings of ASME turbo Expo: Turbomachinery Technical Conference and Exposition, Charlotte, 2017.
[19] Manfrida, G., Pacini L., and Talluri, L., 2017, "A Revised Tesla Turbine Concept for ORC Applications", Energy, Vol. 129, pp. 1055–1062.
[20] Traverso, A., Barberis, S., Larosa, L., and Silvestri, P., 2018, "Reverse Cycle Machine Provided with a Turbine", World Patent WO2018/127445A1
[21] Hasinger, S. H., and Kehrt, L. G., 1963, "Investigation of a Shear-Force Pump", Journal of Engineering for Power, pg. 201-206.